Comparative Investigation on Non-IPR C_{68} and IPR C_{78} Fullerenes Encaging Sc_3N Molecules

Sung Soo Park,[†,‡] Dan Liu,[†] and Frank Hagelberg*[,†]

Computational Center for Molecular Structures and Interactions, Department of Physics, Atmospheric Sciences, and General Science, Jackson State University, Jackson, Mississippi 39217, and Computer Aided Engineering Group, Samsung Electro-Mechanic Co. Ltd, Suwon, South Korea

Received: March 30, 2005; In Final Form: June 8, 2005

A computational study on the experimentally detected $Sc_3N@C_{68}$ cluster is reported, involving quantum chemical analysis at the B3LYP/6-31G* level. Extensive computations were carried out on the pure C_{68} cage which does not conform with the isolated pentagon rule (IPR). The two maximally stable C_{68} isomers were selected as initial $Sc_3N@C_{68}$ cage structures. Full geometry optimization leads to a confirmation of an earlier assessment of the $Sc_3N@C_{68}$ equilibrium geometry (*Nature* **2000**, *408*, 427), namely an eclipsed arrangement of Sc_3N in the C_{68} 6140 frame, where each Sc atom interacts with one pentagon pair. From a variety of theoretical procedures, a D_{3h} structure is proposed for the free Sc_3N molecule. Encapsulated into the C_{68} enclosure, this unit is strongly stabilized with respect to rotation within the cage. The complexation energy of $Sc_3N@C_{68}$ cage is found to be in the order of that determined for $Sc_3N@C_{80}$ and exceeding the complexation energy of $Sc_3N@C_{78}$. The cage−core interaction is investigated in terms of electron transfer from the encapsulated trimetallic cluster to the fullerene as well as hybridization between these two subsystems. The stabilization mechanism of $Sc_3N@C_{68}$ is seen to be analogous to that operative in $Sc_3N@C_{78}$. For both cages, C_{68} and C_{78}, inclusion of Sc_3N induces aromaticity of the cluster as a whole.

I. Introduction

Encapsulating metal atoms into fullerene enclosures gives rise to novel phenomena of relevance for the fundamentals of cluster science as well as technological application.[1] Thus, it has been found that the cage structures of endohedral metallofullerenes may differ from the most stable geometries of the respective pure cages, as observed for composites based on C_{80} [2] and C_{82}.[3] Numerous applications of metallofullerenes in the fields of nanoscale materials science, photochemistry and biomedical technology are envisaged.[4,5] For instance, recent experimental studies suggest that fullerene cages enclosing gadolinium atoms may be utilized as highly effective and biocompatible magnetic resonance imaging (MRI) contrast agents.[6]

H. C. Dorn and co-workers recently discovered novel metallofullerenes of composition $M_xSc_{3-x}N@C_{68}$ with M = La, Gd, Ho, Er, and Tm and $x = 0-2$.[7,8] It is among the interesting features of this newly characterized family of metallofullerenes that they do not conform with the *isolated pentagon rule* (IPR) that has served as a valuable heuristic principle in exploring pure fullerene clusters.[9] This rule states that the most stable fullerenes correspond to structures in which the pentagons are entirely surrounded by adjacent hexagons. The reason for the deviation from this rule as observed for metallofullerenes based on C_{68} is purely topological: Only fullerenes C_N with $N \geq 70$ admit isolated pentagons, excepting C_{60}. Therefore, all possible C_{68} cages based on five and six-membered rings contain adjacent, or "fused" pentagons. The non-IPR unit $Sc_2@C_{66}$ that has been described recently in the literature[10] represents a case comparable to $M_xSc_{3-x}N@C_{68}$. Within the latter cluster family, the species $Sc_3N@C_{68}$ has been detected with particularly high abundance.[7] The NMR spectrum of this metallofullerene was found to be compatible with 11 cage structures combined of pentagon and hexagon rings, all of them characterized by D_3 or S_6 symmetry, and chosen from a set of 6332 possible isomers, as generated by the spiral algorithm.[11] The minimal number of fused pentagon pairs in these selected C_{68} cages turned out to be three. A first tight binding density functional theory (DFT) calculation[12] singled out two cages, labeled 6140 and 6275, as maximally stable within the pool of the 11 competitors. Combining ^{13}C NMR spectroscopy measurements with energy minimization arguments, a unique structure consisting of three fused pentagon pairs with D_3 symmetry was identified as the most likely geometry for the cage of $Sc_3N@C_{68}$. This structure, exhibiting the smallest possible number of pentagon pairs, is in keeping with the pentagon adjacency penalty rule (PAPR).[13] According to this rule, maximally stable non-IPR cages contain the minimal number of fused pentagons since each [5:5] junction enhances the ring strain of the cluster as a whole.[14]

The initial assessment of the preferred $Sc_3N@C_{68}$ geometry was supported by X-ray spectroscopy on $Sc_3N@C_{68}\cdot[Ni^{II}(OEP)]\cdot 2C_6H_6$ crystals[8] from which the structure displayed in Figure 1a emerged as the most probable candidate for the ground-state equilibrium geometry. In this unit, the Sc_3N core is planar, and each Sc atom is located above the midpoint of a pentalene motif of the cage, more specifically the center of the [5:5] junction, i.e., the bond shared between two fused pentagons.

Two further members of the metallofullerene series $Sc_3N@C_N$ have been reported, namely with $N = 78$[15] and $N = 80$.[2c] The cages of both species conform with the IPR rule. For $Sc_3N@C_{78}$, spectroscopy yielded an equilibrium geometry closely related to that proposed for $Sc_3N@C_{68}$ (see Figure 1b). As a marked

* Corresponding author.
† Jackson State University.
‡ Samsung Electro-Mechanic Co. Ltd.

10.1021/jp0516339 CCC: $30.25
Published on Web 09/13/2005

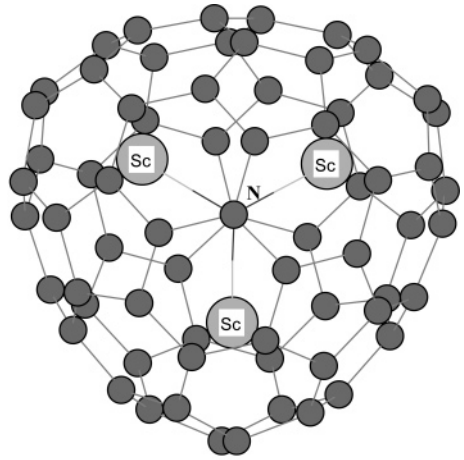

(a) $Sc_3N@C_{68}$

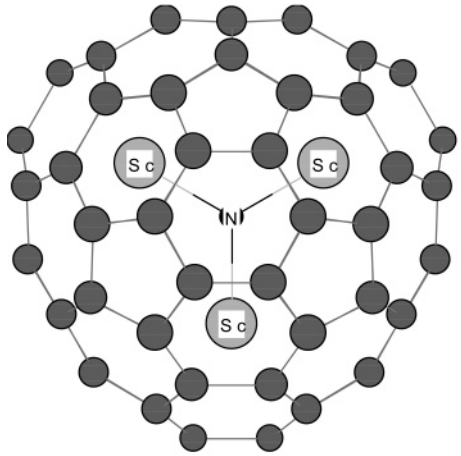

(b) $Sc_3N@C_{78}$

Figure 1. Equilibrium structures of $Sc_3N@C_{68}$ (a) and $Sc_3N@C_{78}$ (b).

difference between the two units, however, each Sc atom of $Sc_3N@C_{78}$ occupies a position above the junction between two adjacent hexagons, while Sc in $Sc_3N@C_{68}$ attaches to pentagon pairs. The structural observations on the former species were confirmed by the computational work of Campanera et al.[16] on the basis of geometry optimizations performed by use of the local spin density approximation (LSDA).[17] The experimentally identified D_{3h} geometry of $Sc_3N@C_{78}$ was found to be most stable within the series of investigated isomers. For $Sc_3N@C_{80}$, I_h symmetry was found which is remarkable since the I_h isomer of the C_{80} cage has been determined by computation to be the least stable among all C_{80} species that satisfy the IPR.[18] The cage symmetry of metallofullerenes, however, may deviate substantially from that of the respective empty cage. Since sizable electron transfer between the trimetallic core and the fullerene enclosure has been recorded for both species, $Sc_3N@C_{78}$ and $Sc_3N@C_{80}$,[16] resulting in a formal charge of -6 au on the cage, it is misleading to compare the neutral fullerene with the metallofullerene cage. Indeed, it has been shown that the hexaanionic I_h isomer of C_{80} unit is of substantially higher stability in relation to the competing isomers than the neutral I_h C_{80} cluster.[19] It is noteworthy that the Sc_3N molecule in C_{78} is strongly stabilized in the position shown in Figure 1b while in C_{80}, it has been found to be free to rotate.

In this work, we present the first computational investigation of the $Sc_3N@C_{68}$ cluster. The emphasis of this effort is on the understanding of the interaction between the encapsulated metal cluster core and the fullerene enclosure. In these investigations, the IPR system $Sc_3N@C_{78}$ provides a natural reference for comparison.

II. Computational Details

All species considered in this work have been subjected to quantum chemical analysis by density functional theory (DFT) using the B3LYP hybrid density functional method in conjunction with the d polarized 6-31G* basis set implemented in the Gaussian 98 program.[20−22] Each unit reported here was fully optimized without symmetry constraints, taking into account all electrons. The structures resulting from geometry optimization have been classified as local minima or stationary points on their respective potential energy surfaces according to the number of their imaginary frequencies. The frequency analysis has been performed at the B3LYP/3-21G level, as necessitated by the considerable sizes of the systems analyzed in this work. For selected clusters, however, the results of the B3LYP/3-21 approach were reexamined by a subsequent computation at the B3LYP/6-31G* level. Thus, both methods confirmed the staggered $Sc_3N@C_{68}$(6275) structure (see subsection IIIc) as a transition state. A variety of DFT, ab initio and hybrid procedures was employed to assess the ground-state geometry of the cluster Sc_3N.

For the composites $Sc_3N@C_{68}$ and $Sc_3N@C_{78}$, complexation energies, i.e., adiabatic binding energies between the cage and the trimetallic core, were computed as the release of energy upon incorporation of the endohedral cluster into the fullerene enclosure according to

$$E_{\mathrm{cmplx}}(\mathrm{Sc_3N@C_N}) = E(\mathrm{Sc_3N@C_N}) - E(\mathrm{Sc_3N}) - E(\mathrm{C_N})$$

The fullerenes C_{68} and C_{78}, the corresponding endohedral clusters $Sc_3N@C_N$ with $N = 68$, 78 and several species of the form $C_{14}H_8$ have been investigated with respect to aromaticity. For this purpose, the nucleus independent chemical shift (NICS)[23] was evaluated at the centers of all inequivalent six membered and five membered rings of the studied species. The calculations were carried out by use of the gauge-independent atomic orbital (GIAO) method.[24]

The natural atomic charges were calculated at the B3LYP/6-31G* level with the natural bond orbital (NBO) program[25] implemented in the Gaussian 98 package.

III. Results and Discussion

In this section, we will comment first on our results on the pure C_{68} cage. Subsequently, we will present our findings on the isolated core molecule Sc_3N, to be followed by a discussion of the composites $Sc_3N@C_{68}$ and $Sc_3N@C_{78}$, with special emphasis on the comparison between these two species.

a. The Pure C_{68} Cage. The 11 C_{68} structures singled out by mass spectrometry in combination with NMR measurement[7] are compatible with either a D_3 or S_6 symmetry assignment. Utilizing the spiral algorithm, one finds 11 structures that satisfy this condition.[11] The previous optimization of these units at the DFT tight binding level[12] has been repeated by use of the B3LYP/3-21G and B3LYP/6-31G* procedures. Energetic properties of the 11 C_{68} isomers are summarized in Table 1. As in the previous analysis by Stevenson et al.,[7] the two units that share a regular arrangement of three fused pentagons, labeled *6140* and *6275*, turn out to be maximally stable within this group. In keeping with the PAPR, both of these clusters contain three pairs of fused pentagons. Their equilibrium structures are shown in Figure 2. The total energies of these two clusters are

TABLE 1: Relative Energies, Lowest Vibrational Frequencies, and Point Groups (PG) of the Eleven C_{68} Cages Considered in This Work, As Evaluated at the B3LYP/6-31G* and 3-21G Levels[d]

isomers	PG	relative energy 3-21G	relative energy 6-31G*	ω^a	HOMO−LUMO gap[b] [degeneracy][c]
6140	D_3	0.0	0.0	222	1.264 [2/2]
6275	D_3	0.45	0.78	214	1.301 [1/1]
6059	D_3	1.31	1.49	211	1.338 [1/1]
6263	S_6	2.38	2.57	212	1.581 [2/2]
6015	D_3	2.41	2.68	212	1.339 [1/2]
2189	D_3	3.11	3.44	191	1.135 [1/1]
3862	D_3	4.16	4.68	199	1.994 [2/1]
3875	D_3	4.39	4.85	197	1.434 [1/2]
3093	D_3	5.34	5.59	189	1.280 [2/1]
3993	D_3	10.03	10.84	196	1.216 [1/1]
663	D_3	10.86	11.85	177	1.489 [1/1]

[a] Lowest frequencies as obtained at the B3LYP/3-21G level. [b] Calculated at the 6-31G* level. [c] [degeneracy of HOMO/degeneracy of LUMO]. [d] All energies are in eV. All structures have been found to be stable from frequency analysis at the 3-21G level.

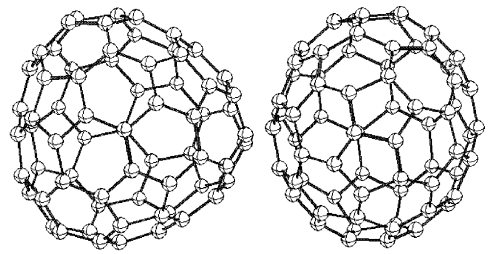

$C_{68}(6140)$ - D_3

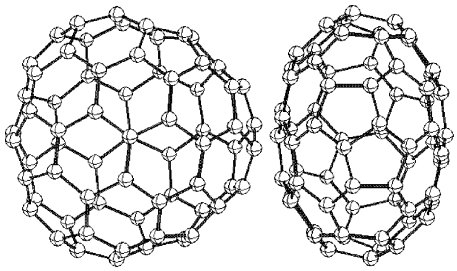

$C_{68}(6275)$ - D_3

Figure 2. Equilibrium structures of the two C_{68} cages found maximally stable, labeled *6140* and *6275*.

separated by a difference of 0.78 according to our B3LYP/6-31G* calculation (0.45 eV as the 3-21G basis set is employed), while the earlier computation yielded 1.24 eV.[12] Although the stability difference between the two competitors is markedly lower in the present than in the previous assessment, isomer 6140 still emerges as the lowest energy structure by a pronounced margin. Comparing our results obtained with the 3-21G and the 6-31G* basis set we note that the differences pertaining to geometry are negligible. The relative energies ΔE, however, show deviations between the approaches which average 12%. The more sizable basis set leads consistently to higher values of ΔE than the smaller one.

b. The Free Sc_3N Molecule. A previous computational investigation on the free Sc_3N molecule yielded a pyramidal C_{3v} geometry with an Sc−N equilibrium bond length of 1.957 Å and an Sc−N−Sc bond angle of 99.1°.[16] In this work, the local spin density approximation[25] was used with the Vosko−Wilk−Nusair (VWN)[26] parametrization for correlation and with Becke[27] and Perdew[28] nonlocal corrections. The C_{3v} symmetry assignment for the free cluster species implies that the interaction between the fullerene cage and the Sc_3N core molecule changes the shape of this molecule from pyramidal to planar, since planar geometry has been established by X-ray analysis for the core of $Sc_3N@C_{68}$, $Sc_3N@C_{78}$, and $Sc_3N@C_{80}$.[2c,8,15] From the computations presented here, however, the structural modification of the Sc_3N by the fullerene cage does not appear to be a cogent conclusion. Performing a geometry optimization of the pure Sc_3N by use of the B3LYP/6-31G* method adopted in our work on the endohedral composite, we arrive at a planar D_{3h} structure, in contrast to the earlier finding. The Sc_3N C_{3v} pyramid results as unstable in spin singlet condition. Examining the C_{3v} spin triplet, we find stability; however, this isomer turns out to be higher in total energy than the spin singlet by the considerable margin of 1.13 eV. To clarify the ambiguous situation with respect to the equilibrium geometry of the free Sc_3N unit, we carried out further calculations, employing a large range of different quantum chemical procedures in conjunction with a variety of basis sets. Our findings are summarized in Table 2. Some trends pervading the data listed in this table can be identified, related to the employed computational technique, i.e., a pure DFT approach, a hybrid or a pure ab initio method.

TABLE 2: Comparison of Sc_3N in D_{3h} and C_{3v} Symmetry As Obtained by Various Quantum Chemical Procedures[k]

method	energy (kcal/mol) D_{3h}	energy (kcal/mol) C_{3v}	natural charge D_{3h} N	natural charge D_{3h} Sc	natural charge C_{3v} N	natural charge C_{3v} Sc
HF/TZV	0.0 (0)		−2.19	0.73		
MP2[a]/TZV	0.0 (0)		−2.19	0.73		
MP2/6-311+G(3df)	0.0 (0)		−2.26	0.75		
MP2/6-31G(d)	0.0 (0)		−2.19	0.73		
QCIS(T)[b]/TZV	0.0 (0)		−2.19	0.73		
B3[c]-LYP[d]/TZV	0.0 (0)		−1.68	0.56		
B3LYP/6-311+G(3df)	0.2 (0)	0.0 (0)	−1.77	0.59		
B3LYP/6-31G(d)	0.0 (0)		−1.71	0.57		
B3−P86[e]/TZV	0.0 (0)		−1.67	0.56		
B3−PW91[f]/TZV	0.0 (0)		−1.68	0.56		
S−VWN/TZV	11.0 (3)	0.0 (0)	−1.51	0.50	−1.40	0.47
SVWN/6-311+G(3df)	16.5 (3)	0.0 (0)	−1.59	0.53	−1.50	0.50
SVWN/6-31G(d)	9.7 (1)	0.0 (0)	−1.55	0.52	−1.49	0.50
S[j]-LYP/TZV	8.2 (3)	0.0 (0)	−1.51	0.50	−1.40	0.47
S−P86/TZV	9.4 (1)	0.0 (0)	−1.51	0.50	−1.40	0.47
S−PW91/TZV	10.5 (1)	0.0 (0)	−1.52	0.51	−1.40	0.47
B[g]-LYP/TZV	7.0 (3)	0.0 (0)	−1.55	0.52	−1.45	0.48
BLYP/6-311+G(3df)	11.9 (3)	0.0 (0)	−1.65	0.55	−1.57	0.52
BLYP/6-31G(d)	5.7 (3)	0.0 (0)	−1.60	0.53	−1.55	0.52
B−P86/TZV	8.4 (3)	0.0 (0)	−1.56	0.52	−1.44	0.48
B−PW91/TZV	9.6 (3)	0.0 (0)	−1.56	0.52	−1.44	0.48
B−VWN[h]/TZV	9.9 (3)	0.0 (0)	−1.55	0.52	−1.43	0.48
B−VWN5[i]/TZV	8.8 (3)	0.0 (0)	−1.56	0.52	−1.44	0.48

[a] MP2: Møller−Plesset correlation energy correction, truncated at the second order.[29] [b] QCIS(T): Quadratic CI calculation including single and double substitutions with a triples contribution to the energy added.[30] [c] B3: Becke's three parameter functional.[20] [d] LYP: the correlation functional of Lee, Yang, and Parr, which includes both local and nonlocal terms.[22] [e] P86: the nonlocal correlation functional provided by the Perdew 86 expression.[31] [f] PW91: Perdew and Wang's 1991 gradient-corrected correlation functional.[32] [g] Becke's one parameter hybrid functional with his 1996 correlation function.[33] [h] VWN: Vosko Wilk Nusair correlation functional fitting the RPA solution to the uniform electron gas, often referred to as Local Spin Density (LSD) correlation.[26] [i] VWN 5: the Vosko Wilk Nusair functional, as obtained from a fit of the Ceperley-Alder solution to the uniform electron gas.[26] [j] S: Slater Local Spin Density exchange, with a coefficient of 2/3.[k] In each case, the number of imaginary frequencies is given in parentheses behind the relative energy. The ground state energy is set to zero. Wherever no optimization result has been obtained, the respective entry is left blank. Ab initio procedures are distinguished by boldface type, and hybrid methods by italic type. The remaining procedures are DFT variants.

In particular, we notice the following features: (1) Without exception, the pure DFT procedures yield stability for the C_{3v} structure while all optimization results for the D_{3h} alternative lead to stationary points, in most cases with as much as three imaginary frequencies. (2) For the hybrid methods, a hybrid picture arises. More specifically, we find a pronounced basis set dependence in this case. Uniform behavior results from the use of the *triple-ζ* valence (TZV) and the 6-31G* basis set. In all of these cases, the D_{3h} geometry emerges as stable while no convergence is reached for C_{3v} symmetry. This changes as one moves to the 6-311+G(3df) basis, i.e., the basis set of highest complexity employed in the context of this work. Utilizing this basis in combination with the B3LYP method one finds both alternatives stable and near-degenerate with a difference in total energy of 0.2 kcal/mol. (3) The full ab initio approach, where the MP2 procedure has been combined with the three basis sets considered here, yields stability for the D_{3h} geometry throughout. As in point 2, the optimizations performed for the C_{3v} isomer do not converge for any of the bases except for that of highest complexity. Here, however, we observe that the initial C_{3v} geometry deforms to relax eventually into the planar D_{3h} shape. (4) The three classes of methods considered here, ab initio, hybrid, and DFT, yield clearly distinct values for the natural charges on the N or Sc atoms. The most sizable electron transfer between Sc and N is obtained from the ab initio, the lowest from the DFT computations. (5) The three computational approaches lead to strongly deviating density of states (DOS) distributions around the Fermi level. This is demonstrated in Figure 3 which compares the total DOS distributions yielded by calculations at the MP2/TZV, the B3LYP/TZV and the S-VWN/TZV level for Sc_3N in D_{3h} symmetry. The energy gap is high for the ab initio procedure, intermediate for the hybrid method, and vanishing for DFT.

As the analyzed system exhibits a substantial amount of electron transfer, and thus charge localization, it may be described more adequately by ab initio and hybrid procedures than by DFT. This consideration suggests a planar D_{3h} geometry as the equilibrium structure of the free Sc_3N unit, implying that Sc_3N does not undergo a change of symmetry as it is incorporated into the fullerene cage. We want to emphasize that the B3LYP procedure yields a consistent result when applied to the Sc_3N (D_{3h}) structure, predicting stability for all of the basis sets employed in this work, with a small variation of the N−Sc bond length on the order of less than 1%. Also, its results are in agreement with those of the most accurate methods used in the present context, namely the MP2/6-311+G(3df) and QCIS(T)/TZV procedures. It is worth while emphasizing that the three classes of computational methods compared above converge in their prediction of a planar Sc_3N core of $Sc_3N@C_N$ with N = 68, 78, 80.

c. $Sc_3N@C_{68}$ and $Sc_3N@C_{78}$. For the two C_{68} cages of minimal energy, labeled *6140* and *6275* in Table 1, we performed full optimizations of $Sc_3N@C_{68}$ using the B3LYP method in conjunction with the 6-31G* and 3-21G basis sets. In each case we adopted an eclipsed as well as a staggered structure as initial geometry. The terms "eclipsed" and "staggered" refer here to the geometric relation between the three Sc atoms of the core and the three fused pentagons of the cage, as shown in Figure 4 which displays two different perspectives on both geometric alternatives for both cages. The staggered initial structure is generated from the eclipsed by rotation of the Sc_3N molecule by 60° about the 3-fold symmetry axis of the cluster. Both clusters share D_3 symmetry. From our computations, an eclipsed arrangement of Sc_3N in the *6140* C_{68}

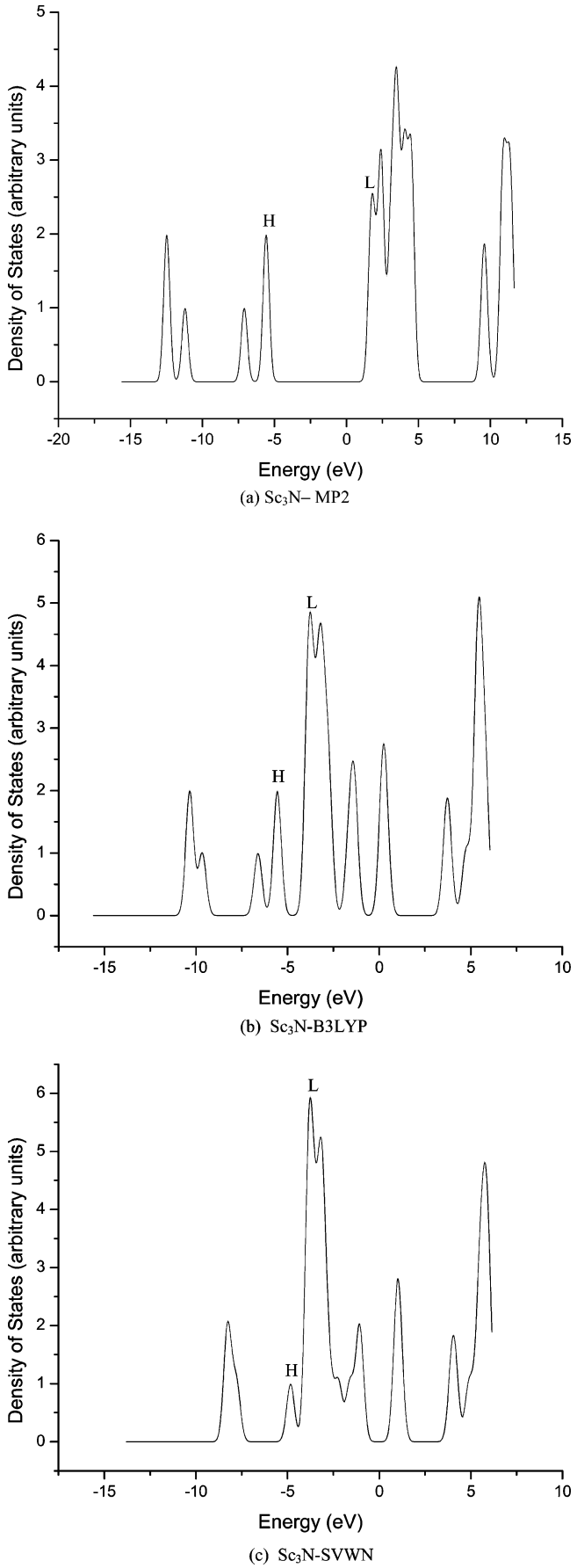

Figure 3. Total density of states (DOS) for Sc_3N at D_{3h} symmetry as emerging from MP2/TZV (a), B3LYP/TZV (b), and S-VWN/TZV (c) computations. The arrows point to the HOMO (H) and LUMO (L) levels.

(a) $Sc_3N@C_{68}$ (6140)

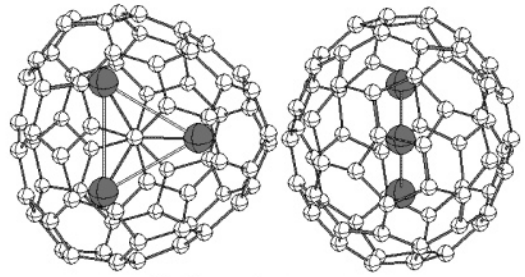

Eclipsed structure

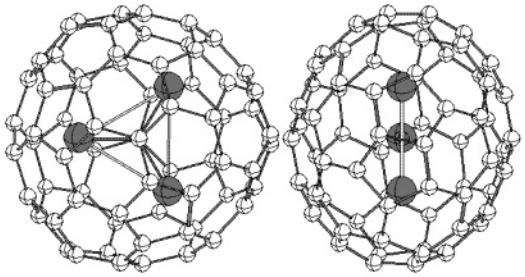

Staggered structure

(b) $Sc_3N@C_{68}$ (6275)

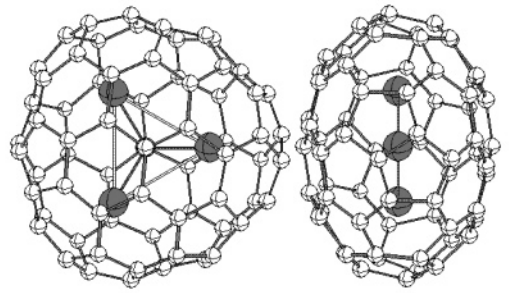

Eclipsed structure

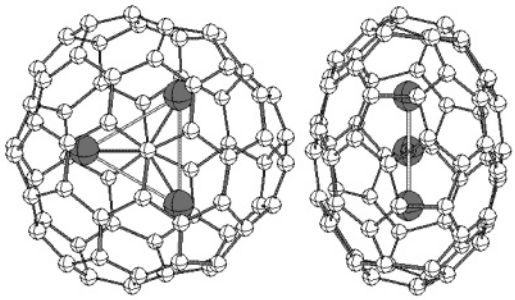

Staggered structure

Figure 4. Investigated geometries of $Sc_3N@C_{68}$ for the *6140* (a) and the *6275* (b) fullerene cage. The eclipsed structures are stable isomers, the staggered alternatives saddle points of third (a) and first (b) order.

frame results as the structure of highest stability (see Figure 4a). Characteristically, each Sc atom in this cluster is oriented toward one pentagon pair. Figure 5 shows a fragment of the cluster of highest stability. The presented substructure consists of the Sc_3N core combined with the pentagon pairs of the C_{68} cage. From the indicated bond lengths it can be seen that the Sc_3N unit undergoes a small bond elongation of 4% when

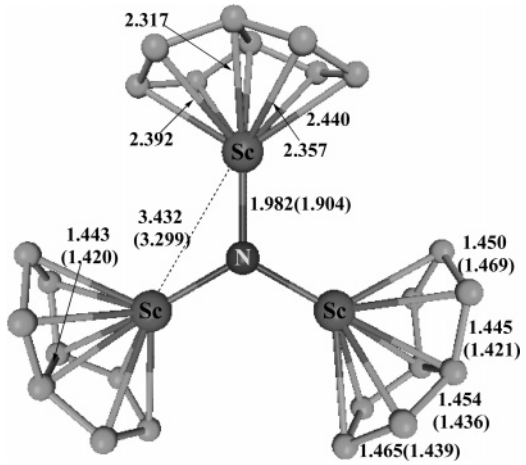

Figure 5. Fragment of the of $Sc_3N@C_{68}$ (6140) ground-state structure, showing the Sc_3N cluster with pentalene-like ligands.

encapsulated into C_{68}; the corresponding increase of C−C distances in the shown cage fragment averages to about 5%. It should be noted that the obtained N−Sc equilibrium bond length in $Sc_3N@C_{68}$ is in keeping with the results of X-ray measurements performed on this metallofullerene.[7] These investigations yielded an average value of 1.98 Å for this quantity. Our finding of d(N−Sc) = 1.982 Å agrees perfectly with the experimental bond length.

The analogous minimum for the *6275* C_{68} cage with enclosed Sc_3N is separated from the ground-state candidate by a large difference in total energy of 4.24 eV. In this case, the N−Sc bond stretching is somewhat more pronounced, amounting to 6%, while the deviation of the C−C distances in the C_8 fragments adjacent to the Sc atoms is found to be 4% on the average. All optimized structures were subjected to frequency analysis at the B3LYP/3-21G level, verifying that both eclipsed structures are true minima. The staggered structures, in contrast, result as stationary points of third and first order for the $Sc_3N@C_{68}$ complexes based on the C_{68} cages *6140* and *6275*, respectively. For the former unit, we find a markedly higher energy difference between the eclipsed and the staggered alternative than for the latter, i.e., 4.52 vs 0.622 eV. While the Sc_3N core is well stabilized with respect to rotation within the cages about their 3-fold axes, this effect is more pronounced for the proposed $Sc_3N@C_{68}$ ground-state equilibrium structure than for its less stable competitor.

An alternative *6140* based structure, which is intermediate between the eclipsed and the staggered alternative, was investigated as well. In this C_3 geometry, the Sc atoms are positioned at "particle sites" , as they locate above one of the two C atoms shared by the fused pentagons. The respective hypothetical geometry, however, was found to converge toward the eclipsed minimum, emphasizing once more the strong stabilization of Sc_3N with respect to rotation within the fullerene enclosure. While the C_3 unit could not be confirmed as an isomer of $Sc_3N@C_{68}$, its counterpart for $Sc_3N@C_{78}$ has been identified,[16] being separated from the ground-state energy of the latter species by the small margin of 0.1 eV.

The substantial stability of the eclipsed geometry of Sc_3N within the 6140 cage is further reflected by its complexation energy E_{cmplx}. We compute for this quantity a high value of −12.07 eV. This may be compared to the result given in ref 16 for the complexation energy of $Sc_3N@C_{78}$ in equilibrium geometry, $E_{cmplx} = -9.73$ eV. To rule out method related uncertainties that could impact the comparison of the two metallofullerenes, we subjected the $Sc_3N@C_{78}$ structure to a

geometry optimization on the basis of the procedure employed in this work, i.e., the B3LYP/6-31G* method with inclusion of all electrons. This computation yielded $E_{cmplx} = -9.62$ eV for $Sc_3N@C_{78}$ which is close to the earlier result. The complexation energy obtained for $Sc_3N@C_{68}$ even exceeds the one calculated for $Sc_3N@C_{80}$, namely -11.6 eV according to ref 16. We note that another computation of $E_{cmplx}(Sc_3N@C_{80})$[35] arrived at a deviating value of -10.72 eV. The latter result was generated by a single point calculation using the B3LYP method applied here; however, the geometry optimization was performed at the BLYP level with basis sets of somewhat reduced size, and thus with a lower degree of accuracy than the calculation of E_{cmplx}. Both results for $Sc_3N@C_{80}$ allow to conclude that the complexation energy of $Sc_3N@C_{68}$ rivals that of $Sc_3N@C_{80}$.

This finding is relevant in the context of a recent experiment,[36] where the differences between complexation energies of the species $Sc_3N@C_N^{z+}$ and $Sc_3N@C_{N-2}^{z+}$, with $N = 78$, 80 and $z = 1$, 2, were determined. The respective values were inferred from measured kinetic energy distributions for unimolecular loss of C_2. Within the experimental accuracy of 0.6 eV, no dependence of the stabilization energy on the fullerene size has been found for these cations. The similarity of the complexation energies for neutral $Sc_3N@C_{68}$ and $Sc_3N@C_{80}$, as established in this work, suggests that a very weak dependence of E_{cmplx} over a sizable interval of fullerene cage sizes, ranging from $N = 68$ to $N = 80$, is indeed conceivable.

The high degree of stabilization experienced by the C_{68} cage upon incorporation of the Sc_3N molecule is rooted in the electronic interaction between the trimetallic core and the fullerene enclosure. This interaction is likely to be dominated by a significant loss of electrons from the core to the cage. Thus, for $Sc_3N@C_N$ with $N = 78$, 80, a formal transfer of six electrons from the Sc atoms to the fullerene enclosure has been reported.[16] Investigating the empty C_{68} *6140* cage and the $Sc_3N@C_{68}$ structure of highest stability with respect to molecular orbital symmetries in the frontier orbital region, we find the sequence $(A_2)(E)(E)$ for the highest occupied and $(E)(E)(A_1)$ for the lowest unoccupied orbitals in the case of the pure C_{68} unit. For $Sc_3N@C_{68}$, the six highest occupied molecular orbitals are labeled $(E)(E)(A_2)(E)(E)(A_1)$, repeating the succession of the low lying virtual orbitals found for C_{68}. This observation is consistent with a formal transfer of six electrons from Sc_3N to C_{68} and thus suggests a similarity between $Sc_3N@C_{68}$ and C_{68} with six added electrons. We followed this idea by performing a full geometry optimization of C_{68}^{6-} at the B3LYP/6-31G* level. The result is a unit of D_3 symmetry. To assess the extent of bond length stretching and thus distortion as one goes from C_{68} to C_{68}^{6-}, we focused on a cage fragment consisting of the pentagon pair and two adjacent hexagons, as shown in Figure 6. We will refer to this cage substructure as a 6−5−5−6 unit and distinguish it in the subsequent discussion from the inverse 5−6−6−5 unit. Figure 6 includes the bond lengths between neighboring C atoms within this motif for three species, namely C_{68}, C_{68}^{6-}, and $Sc_3N@C_{68}$. We note that the average bond elongation from C_{68} to C_{68}^{6-} is found to be 1.33%; from C_{68}^{6-} to $Sc_3N@C_{68}$ it amounts to 0.39%. This demonstrates that the transition from the hexaanionic to the endohedral unit involves a substantially smaller degree of structural distortion than that from the neutral to the hexaanion.

The formal charge assignment $(Sc_3N)^{6+}@C_{68}^{6-}$ is modified by natural charge analysis. Thus, the net natural charge on the cage amounts to -2.95 au. The two polar C atoms, i.e., those that are positioned on the 3-fold axis of the cluster acquire positive charges of 0.031 au while the natural charges of all other C atoms are negative. The difference between the formal and the natural cage charges is indicative of a substantial amount of hybridization between contributions of the Sc_3 subsystem and the cage, as found for the highest occupied orbitals of $Sc_3N@C_{68}$. This observation is in accordance with earlier theoretical work on monometallofullerenes of composition $Sc@C_N$ with $N = 60$ [37] and 82 [38] where strong metal-cage hybridization was reported, related chiefly to the interaction of Sc d valence orbitals with bonding and antibonding π orbitals of the cage. For $Sc_3N@C_{68}$, this feature is reflected by the partial DOS distributions for selected subunits of $Sc_3N@C_{68}$, as shown Figure 7 along with the total DOS. Thus, in the energy interval [−14, −4 eV] adjacent to the HOMO−LUMO gap we find a pronounced representation of fused pentagon contributions accompanied by admixtures of Sc_3. Both components form two separated continua with correlated profiles.

In terms of natural atomic populations, we find that the 4s valence orbital of Sc which is 2-fold occupied in the free Sc

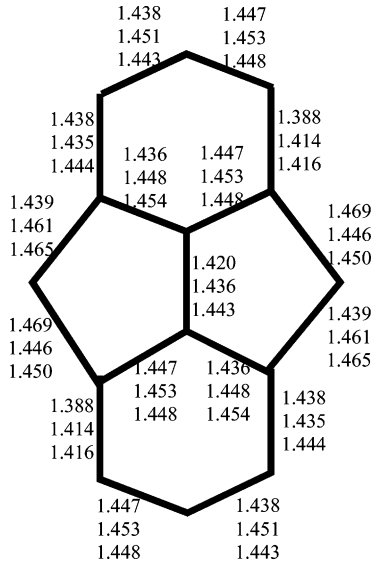

Figure 6. Fragment (6−5−5−6) of the C_{68} cage. For each bond between two C atoms, three bond length values are indicated, denoting the bond length in C_{68} (6140) (highest entry), C_{68}^{6-}, and $Sc_3N@C_{68}$ (lowest entry).

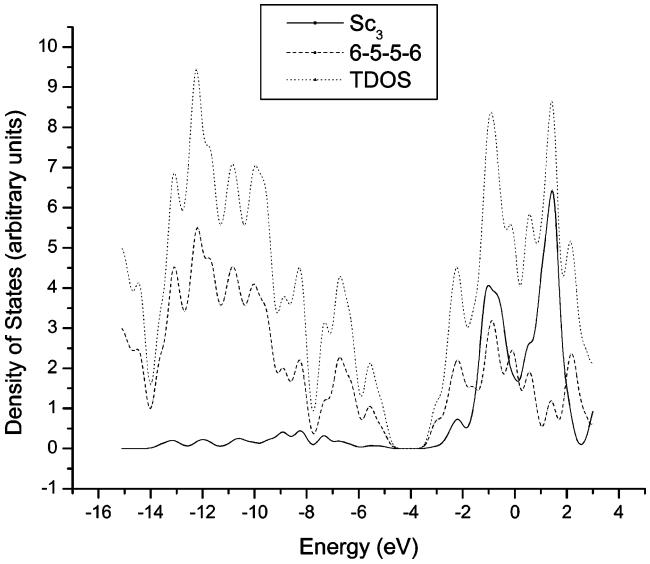

Figure 7. $Sc_3N@C_{68}$ density of states as a function of orbital energy. The total DOS distribution (dotted line) is shown along with the contributions of the C_{14} (6−5−5−6) fragments (dashed line) and of Sc_3 (solid line).

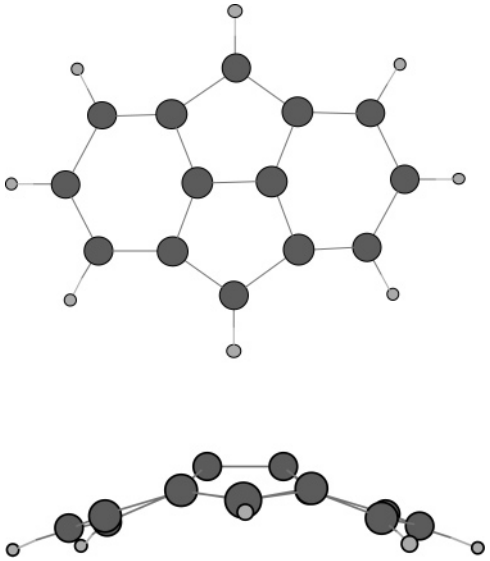

Figure 8. Equilibrium structure of $C_{14}H_8$ (6−5−5−6).

TABLE 3: Relative Energies and Number of Imaginary Frequencies of the $Sc_3N@C_{68}$ Isomers (6140 and 6275) at the B3LYP/6-31G* and 3-21G Levels[c]

isomers		relative energy 3-21G	relative energy 6-31G*	N_{imag}[a]	HOMO−LUMO gap [degeneracy][b]
$Sc_3N@6140$	eclipsed	0.0	0.00	0	2.106 [1/1]
	staggered	4.71	4.52	3	2.394 [2/2]
$Sc_3N@6275$	eclipsed	4.06	4.25	0	1.959 [2/2]
	staggered	4.77	4.87	1	1.881 [2/2]

[a] Numbers of imaginary frequencies, evaluated at the B3LYP/3-21G level. [b] [degeneracy of HOMO/degeneracy of LUMO]. [c] All complexes share D_3 symmetry. The energies are in eVs.

atom, is nearly depleted in $Sc_3N@C_{68}$. From our analysis, only 10% of the original occupation are retained in the 4s orbital, while 27% are transferred to the central N atom and another 14% are promoted from the 4s to the 3d level. The remaining 49% are donated to the cage.

To understand the cage-core interaction mechanisms in greater detail, we considered the 6−5−5−6 motif with terminating H atoms to saturate the dangling C bonds. The 6−5−5−6 cage segments which are in close proximity of the Sc atoms carry the highest charge density on the cage surface. The total natural charge concentrated on these three substructures amounts to 76% of the net charge residing on the cage.

We subjected the planar 6−5−5−6 unit with terminating H atoms, as shown in Figure 8 to optimization at the B3LYP/6-31G* level. Spin singlet conditions were assumed, and the computation was performed for the neutral as well as the dianionic species. The planar D_{2h} units turned out to be unstable as the related geometry optimizations resulted in a stationary point with two imaginary frequencies and a transition state for the neutral unit and the dianion, respectively. Deforming the systems along their unstable coordinates leads to bent isomers of C_{2v} symmetry. As we analyze the two clusters with respect to their energetic properties, we notice a very significant widening of the HOMO−LUMO gap ΔE_{HL} when going from the neutral to the negatively charged unit. Specifically, ΔE_{HL} changes from 1.55 eV for the neutral species to 4.29 eV for the dianion, indicating a substantial stability gain as two electrons are added.

In carbon based ring systems, transition from aromatic to antiaromatic character is frequently seen to be accompanied by a very marked increase of the HOMO−LUMO gap.[39] In view of the pronounced difference of ΔE_{HL} for the 6−5−5−6 complex when stabilized as a neutral and with two added electrons we examined these units under the viewpoint of aromaticity. For this purpose, we adopted the aromaticity criterion proposed by Schleyer.[23] This criterion makes use of a correlation between the ability of a ring structure to sustain a diatropic current and the magnetic shielding at the ring center. In quantitative terms, a negative nucleus independent chemical shift (NICS) at the ring center is indicative of aromaticity. Utilizing this methodology, we computed NICS values for both hexagons and both pentagons of the 6−5−5−6 neutral as well as the dianion. Table 4 lists the NICS values for both species. These values turn out to be consistently positive for the neutral and negative for the dianion, reflecting a distinct change from antiaromatic to aromatic character. We found a similar trend for pure pentalene, i.e., a junction of two pentagons with added terminating hydrogen atoms.

We point out that the 6−5−5−6 ring system is the inverse structure of pyracelene, labeled 5−6−6−5 in the notation adopted here. The latter system turns out to be of interest in the context of $Sc_3N@C_{78}$.[16] It has been shown that in the most stable structure of this composite each Sc atom attaches to a 5−6−6−5 subunit, which is obviously analogous to the interaction between Sc and the 6−5−5−6 motif. From Table 4, no uniquely antiaromatic character can be assigned to the former species as the NICS values found for the hexagons are very close to zero. For the corresponding dianion, however, they are distinctly larger in magnitude and negative throughout. Therefore, both ring systems, 5−6−6−5 and 6−5−5−6, turn out to become aromatic upon addition of two electrons; however, for the former the change of the magnetic screening properties is less marked than for the latter. Correspondingly, we arrive at a less drastic increase of the HOMO−LUMO gap for 5−6−6−5 than 6−5−5−6, determining ΔE_{HL} to be 2.83 eV for the neutral and 3.69 eV for the dianion.

The discussion given in the preceding paragraphs leads naturally to the question for the aromaticity of $Sc_3N@C_N$ with $N = 68, 78$. We thus calculated the NICS values at the centers of the six (seven) inequivalent rings of C_{68} and $Sc_3N@C_{68}$ (C_{78} and $Sc_3N@C_{78}$). For the pure cages, no unanimous assignment

TABLE 4: Nucleus Independent Chemical Shift (NICS) Values at the Centers of Five and Six Membered Rings for Various Systems Discussed in the Text at the GIAO-B3LYP/6-31G* Level

system	no. of NICS centers	NICS values
$C_{14}H_8$ (6−5−5−6)	2	16. 35, 14.85
$C_{14}H_8$ $(6-5-5-6)^{2-}$	2	−13.92, −12.11
$C_{14}H_8$ (5−6−6−5)	2	0.05, 17.04
$C_{14}H_8$ $(5-6-6-5)^{2-}$	2	−20.68, −6.25
C_{68}	6	−8.15, −8.02, −5.26, −3.93, −0.86, −0.17
$Sc_3N@C_{68}$	6	−21.77, −15.24, −12.17, −11.71, −10.36, −8.80
C_{78}	7	−8.84, −8.53, −2.21, −0.97, −0.44, 2.97, 8.96
$Sc_3N@C_{78}$	7	−17.73, −8.58, −7.76, −5.69, −4.35, −3.13, −2.25

TABLE 5: Vertical Ionization Energies, Electron Affinities, and HOMO−LUMO Gaps for the Ground State Structures of C_{68}, Sc_3N, $Sc_3N@C_{68}$, $Sc_3N@C_{78}$, and $C_{14}H_8$ (6−5−5−6 and 5−6−6−5) at the B3LYP/6-31G* Level[a]

system	ionization energy	electron affinity	HOMO−LUMO gap
$C_{14}H_8$ (6−5−5−6)	6.55	1.60	1.55
C_{68}	6.65	3.09	1.26
$Sc_3N@C_{68}$	6.28	1.88	2.09
$C_{14}H_8$ (5−6−6−5)	7.08	0.78	2.83
C_{78}	6.51	2.75	1.54
$Sc_3N@C_{68}$	6.16	1.73	2.27
Sc_3N	5.05	1.14	1.88

[a] All values are in eV.

of aromaticity or antiaromaticity is possible. This is due to the occurrence of extremely small NICS values for C_{68}, while for C_{78} a mixture of positive and negative values is found. Upon implantation of the Sc_3N core, however, an unambiguous picture emerges. Both composites exhibit distinct aromaticity. The corresponding increase of the HOMO−LUMO gap amounts to 0.83 eV for $Sc_3N@C_{68}$ and 0.73 eV for $Sc_3N@C_{78}$, as documented in Table 5.

The vertical ionization energies of both the C_{68} 6140 cage and the $Sc_3N@C_{68}$ composite resemble that of the 6−5−5−6 fragment (see Table 5). The vertical electron affinity of $Sc_3N@C_{68}$ results as a compromise between that of Sc_3N and of C_{68}. With a value of 1.88 eV, this quantity is found to be relatively large, albeit distinctly smaller than the electron affinity of C_{68}. Analogous observations are made for $Sc_3N@C_{78}$ where nevertheless, the ionization energy appears more strongly determined by that of Sc_3N than in the parallel case of $Sc_3N@C_{68}$. We note that the ionization energy and electron affinity values given in Table 5 for C_{78} and $Sc_3N@C_{78}$ are consistently somewhat lower than those reported in ref 16, with about 30%, as found for the electron affinity of $Sc_3N@C_{78}$, as maximum deviation.

IV. Conclusions

In this contribution, the non-IPR composite $Sc_3N@C_{68}$ is analyzed with respect to geometric, energetic and electronic properties by use of the hybrid B3LYP potential. It is further compared with the IPR unit $Sc_3N@C_{78}$. Considering the 11 C_{68} isomers that are consistent with experimental NMR findings,[7] possible structures of $Sc_3N@C_{68}$ were studied for the two most stable cages within this pool of candidates. From these computations, a structure involving an eclipsed arrangement of Sc_3N within the 6140 isomer of C_{68} is proposed as the maximally stable $Sc_3N@C_{68}$ geometry, confirming an earlier assessment[7] as well as an experimental result.[8] As a characteristic feature of the selected complex, each Sc atom is attached to a fused pentagon site, or a 6−5−5−6 cage fragment which is the inverse of the 5−6−6−5 motif that defines the Sc location in the most stable isomer of $Sc_3N@C_{78}$. Rotation of Sc_3N within the C_{68} cage around the 3-fold axis is hindered by a very sizable barrier of 4.52 eV which exceeds the rotational stabilization found in the $Sc_3N@C_{78}$ cluster. Further, the complexation energy of −12.07 eV obtained for $Sc_3N@C_{68}$ surpasses that of $Sc_3N@C_{78}$ by 2.45 eV. Both units, however, exhibit a formal charge transfer of six electrons from the trimetallic core to the fullerene cage. This model is modified by inspection of high lying occupied molecular orbitals which reveals a substantial degree of hybridization between the Sc_3 subunit and the fullerene enclosure. This effect in conjunction with electron transfer to the cage gives rise to aromaticity, as secured for both the $Sc_3N@C_{68}$ and the $Sc_3N@C_{78}$ cluster by NICS calculation.

In continuation of this work, it will be worth while to close the gap between $Sc_3N@C_{68}$ and $Sc_3N@C_{78}$ by theoretical investigations of $Sc_3N@C_N$ with $N = 70$, 72, 74, and 76. This project will be interesting under various aspects. Thus, the high complexation energy found for $Sc_3N@C_N$ with $N = 68$ could indicate a "magical" character of this unit or, in view of the comparable complexation energy reported for $N = 80$, a relatively weak dependence of E_{cmplx} on the cage size for $68 \leq N \leq 80$. This latter possibility is suggested by the recent experiment of Gluch et al.[36] For a more adequate interpretation of this experiment, it will be relevant to perform computations on cationic and dicationic $Sc_3N@C_N$ with $N = 76$, 78, 80.

Further, the present work emphasizes the finding that highly stable complexes can emerge from non-IPR fullerenes. Considering this result in the context of the observation that the PAPR does not necessarily apply to charged cages, as pointed out recently by S. Diaz-Tendero,[40] it is not a priori clear that IPR cages C_N will turn out to be the maximally stable enclosures of Sc_3N in the size region $70 \leq N \leq 76$. Addressing this problem may be helpful for examining the validity of the IPR rule for charged fullerenes or metallofullerenes with pronounced internal charge-transfer characteristics.

Acknowledgment. This work is supported by the National Science Foundation through the grants HRD-9805465, NSFESP-0132618 and DMR-0304036, by the National Institute of Health through Grant S06-GM008047, by the Air Force Office of Scientific Research, Grant No. F49620-02-1-026-0, and by the Army High Performance Computing Research Center under the auspices of Department of the Army, Army Research Laboratory, under Cooperative Agreement No. DAAD 19-01-2-0014.

References and Notes

(1) (a) Heath, J. R.; O'Brien, S. C.; Zhang, Q.; Liu, Y.; Curl, R. F.; Kroto, H. W.; Tittel, F. K.; Smalley, R. E. *J. Am. Chem. Soc.* **1985**, *107*, 7779. (b) Chai, Y.; Guo, T.; Jin, C.; Haufler, R. E.; Chibante, L. P. F.; Fure, J.; Wang, L.; Alford, J. M.; Smalley, R. E. *J. Phys. Chem.* **1991**, *95*, 7564.

(2) (a) Kobayashi, K.; Nagase, S.; Akasaka, T. *Chem. Phys. Lett.* **1996**, *261*, 502. (b) Shimotani, H.; Ito, T.; Iwasa, Y.; Taninaka, A.; Shinohara, H.; Nishibori, E.; Takata, M.; Sakata, M. *J. Am. Chem. Soc.* **2004**, *126*, 364. (c) Stevenson, S.; Rice, G.; Glass, T.; Harich, K.; Cromer, F.; Jordan, M. R.; Craft, J.; Hadju, E.; Bible, R.; lmstead, M. M.; Maitra, K.; Fisher, A. J.; Balch, A. L.; Dorn, H. C. *Nature (London)* **1999**, *401*, 55.

(3) (a) Takata, M.; Umeda, B.; Nishibori, E.; Sakata, M.; Saito, Y.; Ohno, M.; Shinohara, H. *Nature* **1995**, *377*, 46. (b) Yamamoto, E.; Tansho, M.; Tomiyama, T.; Shinohara, H.; Kawahara, H.; Kobayashi, Y. *J. Am. Chem. Soc.* **1996**, *118*, 2293. (c) Takata, M.; Nishibori, E.; Umeda, B.; Sakata, M.; Yamamoto, E.; Shinohara, H. *Phys. Rev. Lett.* **1997**, *78*, 3330. (d) Akasaka, T.; Nagase, S.; Kobayashi, K.; Wälchli, M.; Yamamoto, K.; Funasaka, H.; Kako, M.; Hoshino, T.; Erata, T. *Angew. Chem., Int. Ed. Engl.* **1997**, *36*, 1643. (e) Kobayashi, K.; Nagase, S. *Chem. Phys. Lett.* **1998**, *282*, 325. (f) Sueki, K.; Akiyama, K.; Kikuchi, K.; Nakahara, H. *J. Phys. Chem. B* **1999**, *103*, 1390. (g) Sanakis, Y.; Tagmatarchis, N.; Aslanis, E.; Ioannidis, N.; Petrouleas, V.; Shinohara, H. Prassides, K. *J. Am. Chem. Soc.* **2002**, *123*, 9924.

(4) Shinohara, H. In *Fullerenes: Chemistry, Physics and Technology*; Kadish, K. M., Ruoff, R. S., Eds.; John Wiley & Sons: New York, 2000; p 357.

(5) Shinohara, H. *Rep. Prog. Phys.* **2000**, *63*, 843.

(6) Bolskar, R. D.; Benedetto, A. F.; Husebo, L. O.; Price, R. E.; Jackson, E. F.; Wallace, S.; Wilson, L. J.; Alford, J. M. *J. Am. Chem. Soc.* **2003**, *125*, 5471.

(7) Stevenson, S.; Fowler, P. W.; Heine, T.; Ducham, J. C.; Rice, G.; Glass, T.; Harich, K.; Hadju, F.; Bible, R.; Dorn, H. C. *Nature (London)* **2000**, *408*, 427.

(8) Olmstead, M. M.; Lee, H. M.; Duchamp, J. C.; Stevenson, S.; Marciu, D.; Dorn, H. C.; Balch, A. L. *Angew. Chem., Int. Ed.* **2003**, *42*, 900.

(9) Dresselhaus, M. S.; Dresselhaus, G.; Eklund, P. C. *Science of Fullerenes and Carbon Nanotubes*; Academic Press: San Diego, CA, 1996; p 62.

(10) Wang, C. R.; Kai, T.; Tomiyama, T.; Yoshida, T.; Kobayashi, Y.; Nishibori, E.; Takata, M.; Sakata, M.; Shinohara, H. *Nature* **2000**, *408*, 426.

(11) Fowler, P. W.; Manoloupoulos, D. E. *An Atlas of Fullerenes*; Oxford University Press: Oxford, U.K., 1995.

(12) Seifert, G.; Porezag, D.; Frauenheim, T. *Int. J. Quantum Chem.* **1996**, *58*, 185.

(13) Campbell, E. E. B.; Fowler, P. W.; Mitchell, D.; Zerbetto, F. *Chem. Phys. Lett.* **1996**, *250*, 544.

(14) Albertazzi, E.; Domene, C.; Fowler, P. W.; Heine, T.; Seifert, G.; van Alsenoy, C.; Zerbetto, F. *Phys. Chem. Chem. Phys.* **1999**, *1*, 2913.

(15) Olmstead, M. M.; de Bettencourt-Dias, A.; Duchamp, J. C.; Stevenson, S.; Marciu, D.; Dorn, H. C.; Balch, A. L. *Angew. Chem., Int. Ed*. **2001**, *40*, 1223.

(16) Campanera, J. M.; Bo, C.; Olmstead, M. M.; Balch, C. L.; Poblet, J. M. *J. Phys. Chem. A* **2002**, *106*, 12356.

(17) e.g. Koch, W.; Holthausen, M. C. *A chemist's guide to density functional theory*; Wiley: Weinheim, Germany, 2000; p 72.

(18) Kobayashi, K.; Nagase, S.; Akasaka, T. *Chem. Phys. Lett.* **1995**, *245*, 230.

(19) Fowler, P. W.; Zerbetto, F. *Chem. Phys. Lett.* **1986**, *131*, 144.

(20) Frisch, M. J.; Trucks, G. W.; Schlegel, H. B.; Scuseria, G. E.; Robb, M. A.; Cheeseman, J. R.; Zakrzewski, V. G.; Montgomery, J. A., Jr.; Stratmann, R. E.; Burant, J. C.; Dapprich, S.; Millam, J. M.; Daniels, A. D.; Kudin, K. N.; Strain, M. C.; Farkas, O.; Tomasi, J.; Barone, V.; Cossi, M.; Cammi, R.; Mennucci, B.; Pomelli, C.; Adamo, C.; Clifford, S.; Ochterski, J.; Petersson, G. A.; Ayala, P. Y.; Cui, Q.; Morokuma, K.; Malick, D. K.; Rabuck, A. D.; Raghavachari, K.; Foresman, J. B.; Cioslowski, J.; Ortiz, J. V.; Stefanov, B. B.; Liu, G.; Liashenko, A.; Piskorz, P.; Komaromi, I.; Gomperts, R.; Martin, R. L.; Fox, D. J.; Keith, T.; Al-Laham, M. A.; Peng, C. Y.; Nanayakkara, A.; Gonzalez, C.; Challacombe, M.; Gill, P. M. W.; Johnson, B. G.; Chen, W.; Wong, M. W.; Andres, J. L.; Head-Gordon, M.; Replogle, E. S.; Pople, J. A. *Gaussian 98*, revision A.1; Gaussian, Inc.: Pittsburgh, PA, 1998.

(21) Becke, A. D. *J. Chem. Phys.* **1993**, *98*, 5648.

(22) Lee, C.; Yang, W.; Parr, R. G. *Phys. Rev. B* **1988**, *37*, 785.

(23) von Rague Schleyer, P.; Maerker, C.; Dransfeld, A.; Jiao, H.; van Eikema Hommes, N. J. R. *J. Am. Chem. Soc*. **1996**, *16*, 6317.

(24) e.g. Wolinski, K.; Hilton, J. F.; Pulay, P. *J. Am. Chem. Soc.* **1990**, *112*, 8251.

(25) Carpenter, J. E.; Weinhold, F. *J. Mol. Struct. (THEOCHEM)* **1988**, *169*, 41.

(26) Vosko, S. H.; Wilk, L.; Nusair, M. *Can. J. Phys.* **1980**, *58*, 1200.

(27) Becke, A. D. *J. Chem. Phys.* **1986**, *84*, 4524. Becke, A. D. *Phys. Rev. A* **1988**, *38*, 3098.

(28) Perdew, J. P. *Phys. Rev. B* **1986**, *34*, 7406.

(29) Møller, C.; Plesset, M. S. *Phys. Rev.* **1934**, *46*, 618.

(30) Pople, J. A.; Head-Gordon, M.; Raghavachari, K. *J. Chem. Phys.* **1987**, *87*, 5968.

(31) Perdew, J. P. *Phys. Rev. B* **1986**, *33*, 8822.

(32) Perdew, J. P. *Phys. Rev. B* **1992**, *45*, 13244.

(33) Becke, A. D. *J. Chem. Phys.* **1996**, *104*, 1040.

(34) Schaefer, A.; Horn, H.; Ahlrichs, R. *J. Chem. Phys.* **1992**, *97*, 2571.

(35) Kobayashi, K.; Sako, Y.; Nagase, S. *J. Comput. Chem.* **2001**, *22*, 1353.

(36) Gluch, K.; Feil, S.; Matt-Leubner, S.; Echt, O.; Scheier, P.; T. Maerk, D. *J. Phys. Chem. A* **2004**, *108*, 6990.

(37) Guo, T.; Odom, G. K.; Scuseria, G. E. *J. Phys. Chem.* **1994**, *98*, 7745. Lu, J.; Zhang, X.; Zhao, X. *Chem. Phys. Lett.* **2000**, *332*, 51.

(38) Lu, J.; Zhang, X.; Zhao, X.; Nagase, S.; Kobayashi, K. *Chem. Phys. Lett.*. **2000**, *332*, 219.

(39) E.g.: Minkin, V. I.; Glukhovtsev, M. N.; Simkin, B. Y. *Aromaticity and Antiaromaticity: Electronic and Structural Aspects*; Wiley: New York, 1994.

(40) Diaz-Tendero, S.; Martin, F.; Alcami, M. *ChemPhysChem*. **2005**, *6*, 92.